

Self-Learning for Received Signal Strength Map Reconstruction with Neural Architecture Search

Aleksandra Malkova^{1,2}, Loïc Pauletto^{1,3}, Christophe Villien², Benoît Denis²,
and Massih-Reza Amini¹

¹ Université Grenoble Alpes, LIG-APTİKAL, F-38401 Saint Martin d'Hères, France

² Université Grenoble Alpes, CEA-Leti, F-38000 Grenoble, France

³ Bull/Atos, F-38000 Grenoble, France

Abstract. In this paper, we present a Neural Network (NN) model based on Neural Architecture Search (NAS) and self-learning for received signal strength (RSS) map reconstruction out of sparse single-snapshot input measurements, in the case where data-augmentation by side deterministic simulations cannot be performed. The approach first finds an optimal NN architecture and simultaneously train the deduced model over some ground-truth measurements of a given (RSS) map. These ground-truth measurements along with the predictions of the model over a set of randomly chosen points are then used to train a second NN model having the same architecture. Experimental results show that signal predictions of this second model outperforms non-learning based interpolation state-of-the-art techniques and NN models with no architecture search on five large-scale maps of RSS measurements.

Keywords: Neural Architecture Search · Self-learning · Received Signal Strength · Radio Mapping

1 Introduction

The integration of low-cost sensor and radio chips in a plurality of connected objects in the Internet of Things (IoT) has been contributing to the fast development of large-scale physical monitoring and crowdsensing systems in various kinds of smart environments (e.g., smart cities, smart homes, smart transportations, etc). In this context, the ability to associate accurate location information with the sensor data collected on the field opens appealing perspectives in terms of both location-enabled applications and services [13].

Among possible localization technologies, Global Positioning Systems (GPS) have been widely used in outdoor environments for the last past decades. However, these systems still suffer from high power consumption, which is hardly compliant with the targeted IoT applications.

In order to preserve both nodes' low complexity and fairly good localization performances, an alternative is to interpret radio measurements, such as the Received Signal Strength Indicator (RSSI) (i.e., received power of sensor data packets sent by IoT nodes and collected at their serving base station(s)),

as location-dependent fingerprints for indicating the positions of mobile devices [5,6,8,32,36]. Typical fingerprinting methods applied to wireless localization [34] ideally require the prior knowledge of a complete map of such radio metrics, covering the area of interest. However, in real life systems, it is impractical to collect measurements from every single location of the map and one must usually rely uniquely on sparse and non-uniform field data. In order to overcome this problem, classical map interpolation techniques, such as radial basis functions (RBF) or kriging [7], have been used in this context. These approaches are simple and fast, but they are quite weak in predicting the complex and heterogeneous spatial patterns usually observed in real life radio signals (e.g., sudden and/or highly localized transient variations in the received signal due to specific environmental effects). Data augmentation techniques have thus been proposed for artificially increasing the number of measurements in such radio map reconstruction problems. Typically, once calibrated over a few real field measurements, deterministic prediction tools can generally simulate electromagnetic interactions of transmitted radio waves within the environment of study [16,25,31]. The purpose is then to use the generated synthetic data as additional data to train complex models for map interpolation. However, these tools require a very detailed description of the physical environment and can hardly anticipate on its dynamic changes over time. Their high computational complexity is also a major bottleneck.

In this paper, we consider RSSI map reconstruction in a constrained low-cost and low-complexity IoT context, where one can rely only on few ground-truth (i.e., GPS-tagged) single-snapshot field measurements and for which data-augmentation techniques based on side deterministic simulations cannot be applied, due to their prohibitive computational cost and/or to *a priori* unknown environment physical characteristics. This problem of map interpolation is similar to the task of image restoration for which, NN based models with fixed architectures have been already proposed [33]. In the case where there are few observed pixels in an image these approaches fail to capture its underlying structure that is often complex. To tackle this point we propose a first NN model based on Neural Architecture Search (NAS) for the design of the most appropriate model given a RSSI map with a small number of ground truth measurements. For this purpose, we develop two strategies based on genetic algorithms and dynamic routing for the search phase. We show that with the latter approach, it is possible to learn the model parameters while simultaneously searching the architecture. Ultimately, in order to enhance the model's predictions, the proposed approach uses also some extra data of the map with the predictions of the optimized NN in non-visited positions together with the initial set of ground-truth measurements for learning a final model. The proposed technique thus aims at finding practical trade-offs between agnostic learning interpolation techniques and data-augmented learning approaches based on deterministic prediction tools that generally require a very detailed physical characterization of the operating environment. Experimental results on five large-scale RSSI maps show that our approach outperforms non-learning based interpolation state-of-the-art techniques and NN models with a given fixed architecture.

2 Related work

In this section we report related-work on RSSI map reconstruction, as well as existing techniques proposed for NAS.

2.1 Interpolation techniques

Various spatial interpolation methods have been proposed for radio map reconstruction in the wireless context.

One first approach, known as kriging or Gaussian process regression [18], exploits the distance information between measured points, while trying to capture their spatial dependencies. Another popular method is based on radial basis functions (RBF) [7,9,27]. This technique is somehow more flexible, makes fewer assumptions regarding the input data (i.e., considering only the dependency on the distance) and is shown to be more tolerant to some uncertainty [29]. In [7] for instance, the authors have divided all the points of a database of outdoor RSSI measurements into training and testing subsets, and compared different kernel functions for the interpolation. The two methods above, which rely on underlying statistical properties of the input data (i.e., spatial correlations) and kernel techniques, require a significant amount of input data to provide accurate interpolation results. Accordingly, they are particularly sensitive to sparse initial datasets. They have thus been considered in combination with crowdsensing. In [20] for instance, so as to improve the performance of basic kriging, one calls for visiting new positions/cells where the interpolated value is still presumably inaccurate. A quite similar crowdsensing method has also been applied in [10] after stating the problem as a matrix completion problem using singular value thresholding. In our case though, we can just rely on a RSSI map with few ground truth initial measurements.

Another approach considered in the context of indoor wireless localization relies on both collected field data and an a priori path loss model that accounts for the effect of walls attenuation between the transmitter and the receiver [15]. In outdoor environments, local path loss models (and hence, particularized RSSI distributions) have been used to catch small-scale effects in clusters of measured neighbouring points, instead of using raw RSSI data [23]. However, those parametric path loss models are usually quite inaccurate and require impractical in-site (self-)calibration.

Data-augmentation approaches. One more way to build or complete radio databases relies on deterministic simulation means, such as Ray-Tracing tools (e.g., [16,25,31]). The latter aim at predicting in-site radio propagation (i.e., simulating electromagnetic interactions of transmitted radio waves within an environment). Once calibrated with a few real field measurements, such simulation data can relax initial metrology and deployment efforts (i.e., the number of required field measurements). Nevertheless, these tools require a very detailed description of the physical environment (e.g., shape, constituting materials and dielectric properties of obstacles, walls...). Moreover, they usually require high

computational complexity. Finally, simulations must be re-run again, likely from scratch, each time minor changes are introduced in the environment.

2.2 NN based models trained after data-augmentation

Machine and deep learning approaches have been recently applied for RSSI Map reconstruction. These methods have shown to be able to retrieve unseen spatial patterns with highly localized topological effects and hidden correlations. Until now, these methods have been trained over simulated datasets given by data-augmentation approaches.

In [17], given a urban environment, the authors introduce a deep neural network called RadioUNet, which outputs radio path loss estimates trained on a large set of generated using the Dominant Path Model data and UNet architecture [28]. In another contribution, the authors have shown that using the feedforward neural network for path loss modelling could improve the kriging performance [30], as conventional parametric path loss models admit a small number of parameters and do not necessarily account for shadowing besides average power attenuation.

Besides wireless applications, similar problems of map restoration also exist in other domains. In [37] for instance, the authors try to build topographic maps of mountain areas out of sparse measurements of the altitudes. For this purpose, they use a Generative Adversarial Network (GAN) architecture, where in the discriminator they compare pairs of the input data and the so-called “received” map, either generated by the generator or based on the full true map. Another close problem making extensive use of neural networks is the image inpainting problem, where one needs to restore missing pixels in a single partial image. By analogy, this kind of framework could be applied in our context too, by considering the radio map as an image, where each pixel corresponds to the RSSI level for a given node location. Usually, such image inpainting problems can be solved by minimizing a loss between true and predicted pixels, where the former are artificially and uniformly removed from the initial image. This is however impossible in our case, as only a few ground-truth field measurements can be used.

In contrast to the previous approaches, we consider practical situations where data-augmentation techniques cannot be used mainly because of unknown environment characteristics and computational limitations, and, where there is only a small amount of ground-truth measurements. Our approach automatically searches an optimized Neural Network model for the RSSI map reconstruction in hand, and, it is based on self-training for learning an enhanced NN model with the initial ground-truth and pseudo-labeled measurements obtained from the predictions of the first NN model on a set of randomly chosen points in the map.

2.3 NAS related methods

Studies on the subject of NAS have gained significant interest in the last few years. In the literature; there are various of techniques based on Reinforcement Learning (RL) [38], evolutionary algorithm [26] or Bayesian Optimization (BO) [12]. Recently, new gradient-based methods became increasingly popular. One of the first methods using this technique is called DARTS [22], in which a relaxation is used to simultaneously optimize the structure of a *cell*, and the weight of the operations relative to each *cell*. At the end, cells are manually stacked to form a neural network. Based on DARTS, more complex methods have emerged such as AutoDeepLab [21] in which a network is optimized at 3 levels : (i) the parameters of the operations, (ii) the cell structure and (iii) the macro-structure of the network that is stacked manually. Despite a complex representation leading to powerful architectures, this technique has certain drawbacks, such as the fact that the generated architecture is single-path, which means it does not fully exploit the representation’s capabilities. Moreover, as the search phase is over a fixed architecture, it might not be the same between different runs, thus it is complicated to use transfer learning and the impact of training from scratch can be significant. To overcome these limitations, one technique is to use *Dynamic Routing (DR)* as proposed in [19]. This approach is different from the traditional gradient based methods proposed for NAS in the sense that it does not look for a specific fixed architecture but generates a dynamic path in a mesh of cells on the fly *without searching*.

3 NAS for RSSI map reconstruction

In this section, we first introduce our notations and setting, and then present our main approach, denoted as SL_{NAS} in the following.

3.1 Notations and Setting

For a given base station X , let $Y \in \mathbb{R}^{H \times W}$ be the whole matrix of ground-truth signal measurements, where $H \times W$ is the size of the (discretized) area of interest. We suppose to have access to only some ground truth measurements Y_m in Y , that is $Y_m = Y \odot M$, where $M \in \{0, 1\}^{H \times W}$ is a binary mask indicating whether each pixel includes one available measurement or not, and \odot is the Hadamard’s product. Here we suppose that the number of non-null elements in Y_m is much lower than $H \times W$. We further decompose the measurements set Y_m into three parts Y_ℓ (for *training*), Y_v (for *validation*) and Y_t (for *test*), such that $Y_\ell \oplus Y_v \oplus Y_t = Y_m$, where \oplus is the matrix addition operation. Let X_ℓ, X_v, X_t, X_m be the associated 2D node locations (or equivalently, the cell/pixel coordinates) with respect to base station X and X_u be the set of 2D locations for which no measurements are available.

Our approach is based on three main phases *i) architecture search phase* - the search of an optimal architecture of a Neural Network model; *ii) data-augmentation phase* - the assignment of pseudo-labels to randomly chosen unlabeled data using the predictions of the found NN model trained over Y_ℓ ; and *iii)*

that compute either the average or the maximum on the filter of size 4. Candidate architectures are then built from randomly sampled operations and the corresponding NN models are trained. The 30 resulting architectures are then ranked according to a pixel-wise Mean Absolute Error (MAE) criterion between the interpolated result of the network and the set of interpolated measurements given by RBF \hat{Y}_u . The most performing one is finally selected for mutation and placed in the trained population. The oldest architecture is removed in order to keep the size of the population equal to 20 as in [26]. Figure 1 illustrates such an optimized architecture with 18 nodes, which was found for the RSSI Map of the city of Grenoble used in our experiments (Section 4).

Dynamic Routing (DR) For the training phase, we employ the same structure and routing process as those proposed in [19] (Figure 2). The structure is composed of 4 down-sampling level, where the size of the features map is divided by 2 at each level, but the depth of the latter is multiplied by 2 using a 1×1 2D-convolution. In our experiments we use a networks of 9 layers, which correspond to 33 cells in total (in yellow on Fig.2) . The structure also contains an "upsampling aggregation" module at the end (red part on Fig.2). The goal of this module is to combine the features maps from all levels and reconstruct a map of the size of the input. Different from [19], here, each cells contains three *transforming* operations (i.e. 2D-convolution with a kernel size of 3, 5 or 7) to have a good point of comparison with the method described above. However, due to the structure of the network we decided not to use pooling operations, as this could have been potentially redundant. In addition, we have left the possibility of creating residual connections by adding operation identity in each cells. Moreover, we did not use the first two convolutions, originally used to reduce the size of the input, in order to keep as much information as possible. Instead, we used a 1×1 2D-convolution (in purple on Fig.2).

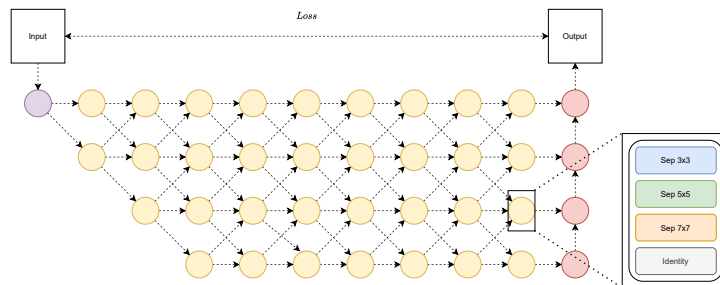


Fig. 2: Diagram of the architecture used in our experiments. The purple, yellow and red dots represents respectively the "stem" convolution, the cells and the "upsampling aggregation" module. The arrows represent the data flow.

3.3 Data-augmentation and Self-Learning phases

After the search phase, the found NN model with parameters θ , f_θ is trained on (X_ℓ, Y_ℓ) by minimizing the following loss :

$$\mathcal{L}(X_\ell, Y_\ell, \theta) = \ell(f_\theta(X_\ell), Y_\ell) + \lambda \|\theta\|_2^2 + \mu \Omega(f_\theta(X_\ell)) \quad (1)$$

where $\ell(\cdot)$ is the Mean Absolute Error (MAE), and $\Omega(f_\theta(X_\ell))$ is the total variation function defined as:

$$\Omega(Z) = \sum_{i,j} |z_{i+1,j} - z_{i,j}| + |z_{i,j+1} - z_{i,j}|,$$

with $z_{i,j}$ the measurement value of a point of coordinates i, j in some signal distribution map Z . This function estimates the local amplitude variations of points in Z that is minimized in order to ensure that neighbour points will have fairly close predicted measurements (i.e., preserving signal continuity/smoothness). Here, λ and μ are hyperparameters for respectively the regularization and the total variation terms and they are found by cross-validation.

With Dynamic routing used in the search phase, we optimize the network structure and the learning of parameters minimizing (Eq. 1) at the same time. Referring to Algorithm 1, the step 1 and 2 are combined in this case.

Let θ_1^* be the parameters of the optimized NN model found by minimizing the loss (1) on ground truth measurements (X_ℓ, Y_ℓ) . This model is then applied to randomly chosen points, $X_u^{(k)}$, in X_u and pseudo-RSSI measurements $\tilde{Y}_u^{(k)}$ are obtained from the predictions of the optimized NN model $f_{\theta_1^*}$: $\tilde{Y}_u^{(k)} = f_{\theta_1^*}(X_u^{(k)})$.

With the same NN architecture, a second model $f_{\theta_2^*}$ is obtained by minimizing the loss (1) over the augmented training set $(X_\ell, Y_\ell) \cup (X_u^{(k)}, \tilde{Y}_u^{(k)})$.

4 Experiments

In this section we will first describe our experimental setup and then present our experimental results.

Experimental Setup. In all experiments, we considered maps of size 368×368 cells and tested our algorithm on field data from two distinct urban environments, namely the cities of Grenoble (France) and Antwerp (The Netherlands). We aggregated and averaged the given measurements in cells/pixels of size 10 meters x 10 meters. The Antwerp dataset is described in detail in [1] on which we considered three base stations, BS'_1 , BS'_2 and BS'_3 , with respectively 5969, 6450 and 7118 ground-truth measurements. For the Grenoble dataset, we collected GPS-tagged LoRa RSSI measurements with respect to 2 base stations located in different sites BS_1 and BS_2 with respectively 16577 and 7078 ground truth measurements. To perform in-cell data aggregation, we measured the distances based on local East, North, Up (ENU) coordinates. Then in each cell, we also computed the mean received power over all in-cell measurements (once

	Grenoble		Antwerp		
	BS_1	BS_2	BS'_1	BS'_2	BS'_3
RBF [4]	5.03 [↓]	3.16 [↓]	3.58 [↓]	3.35	3.90
KRIG [24]	5.68 [↓]	4.21 [↓]	3.69 [↓]	4.39 [↓]	4.91 [↓]
NS [3]	5.11 [↓]	3.14 [↓]	4.28 [↓]	3.45	3.87
TV	5.13 [↓]	2.89	3.76	3.51	3.83
DIP [33]	5.14 [↓]	3.22 [↓]	3.53	3.41	3.92
SL _{NAS} -DR	4.82	2.82	3.48	3.42	3.81
SL _{NAS} -GA($f_{\theta_1^*}$)	4.79	2.81	3.39	3.27	3.75
SL _{NAS} -GA($f_{\theta_2^*}$)	4.76	2.79	3.33	3.27	3.74

Table 1: Average values of the MAE, dB of different approaches on all base stations.

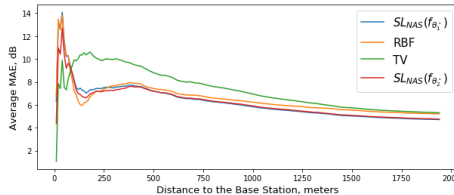


Fig. 3: MAE vs distance to the base station, BS_1 .

converted into RSSI values), before feeding our algorithm and the averaged RSSI values have been normalized between 0 and 1.

For each base station, 8% of the pixels with ground-truth measurements were chosen for training (X_ℓ, Y_ℓ), 2% for validation (X_v, Y_v) and the remaining 90% for testing (X_t, Y_t). The unlabeled data used in **Step 3** of Algorithm 1 were selected at random from the remaining 4% of each map’s cells with no ground truth measurements. Results are evaluated over the test set using the MAE, dB, estimated after re-scaling the normalized values to the natural received signal strength ones. The reported errors are averaged over 20 random sets (training/validation/test) of the initial ground-truth data and unlabeled data were randomly chosen for each experiment.

We compare Radial basis functions (RBF) [4] with linear kernel that were found the most performant, kriging (KRIG) [24], and Navier-Stocks (NS) [3] state-of-the-art interpolation techniques with the proposed SL_{NAS} approach. For the latter, we employ both search phase methods based on Genetic Algorithm (GA) and Dynamic Routing (DR) and respectively referred to as SL_{NAS}-GA and SL_{NAS}-DR. For SL_{NAS}-GA we also evaluate the impact of the self-training step (**Step 3**) (called SL_{NAS}-GA($f_{\theta_2^*}$)) by comparing it with the NN model found at **Step 1** (called SL_{NAS}-GA($f_{\theta_1^*}$)). The evolutionary algorithm in the architecture search phase (Section 3.2) was implemented using the NAS-DIP [11] package⁴. The latter was developed over the Deep Image Prior (DIP) method [33] which is a NN model proposed for image reconstruction. By considering RSSI maps as corrupted images with partially observed pixels (ground-truth measurements), we also compare with this technique by training a NN model having the same architecture than the one presented in [33] and referred to as DIP in the following. All experiments were run on Tesla V100 GPU.

Experimental Results. Table 1 summarizes results obtained on the five considered RSSI maps. We use boldface to indicate the lowest errors. The symbol [↓] indicates that the error is significantly higher than the best result with respect to Wilcoxon rank sum test used at a p -value threshold of 0.01 [35]. In all cases, SL_{NAS}-GA and SL_{NAS}-DR perform better than other state-of-the-art models

⁴ <https://github.com/Pol22/NAS-DIP>

even without the data-augmentation and self-training steps ($\text{SL}_{\text{NAS-GA}}(f_{\theta_1^*})$). We notice that DIP which is also a NN based model but with a fixed architecture has similar results than RBF. These results show that the search of an optimized NN model is effective for RSSI map reconstruction in a constrained low-cost and low-complexity IoT context.

Figure 3 depicts the average MAE in dB with respect to the distance to the Base Station BS_1 for the city of Grenoble. For a distance above 250m, $\text{SL}_{\text{NAS-GA}}(f_{\theta_2^*})$ provides uniformly better predictions in terms of MAE. These results suggest further investigations for a better analysis of the model’s predictions with respect to signal dynamics in regions where the signal is more erratic and where the dynamics is high in the case where additional contextual knowledge about the physical environment can be added in the learning process (e.g., typically as a side information channel or the city map).

Figure 4 displays the MAE, dB boxplots of DIP, RBF and $\text{SL}_{\text{NAS-GA}}(f_{\theta_2^*})$ on BS_1 for different percentages of unlabeled data used in the self-learning phase (Section 3.3). We notice that by increasing the size of unlabeled examples, the variance of MAE for $\text{SL}_{\text{NAS-GA}}(f_{\theta_2^*})$ increases mostly due to the increase of noisy predicted signal values by $f_{\theta_1^*}$. This is mostly related to learning with imperfect supervisor that has been studied in semi-supervised learning [2,14]. As future work, we plan to incorporate a probabilistic label-noise model in **step 3** of algorithm 1 and to learn simultaneously the parameters of the NN and the label-noise models.

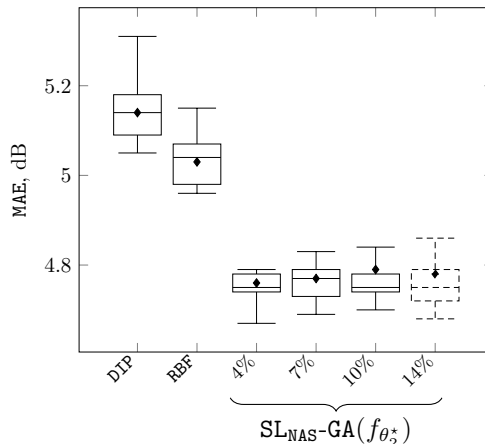


Fig. 4: Boxplots showing the MAE, dB distributions of DIP, RBF and $\text{SL}_{\text{NAS-GA}}(f_{\theta_2^*})$ on BS_1 for different percentage of unlabeled data $\{4, 7, 10, 14\}$ used in the self-learning phase.

5 Conclusion

In this article, we presented a Neural Network model based on NAS and self-learning for RSS map reconstruction from sparse single-snapshot input measurements in the absence of data augmentation via side deterministic simulations. We presented two variants for the search phase of NAS based on Genetic algorithm and Dynamic routing. Experimental results on five large-scale maps of RSS measurements reveal that our approach outperforms non-learning based interpolation state-of-the-art techniques and NN with manually designed architecture.

References

1. Aernouts, M., Berkvens, R., Vlaenderen, K.V., Weyn, M.: Sigfox and lorawan datasets for fingerprint localization in large urban and rural areas. *Data* **3**(2) (2018)
2. Amini, M.R., Usunier, N., Laviolette, F.: A transductive bound for the voted classifier with an application to semi-supervised learning. In: *Advances in Neural Information Processing Systems*. pp. 65–72 (2009)
3. Bertalmio, M., Bertozzi, A.L., Sapiro, G.: Navier-stokes, fluid dynamics, and image and video inpainting. In: *CVPR* (2001)
4. Bishop, C.M.: *Pattern Recognition and Machine Learning (Information Science and Statistics)*. Springer-Verlag, Berlin, Heidelberg (2006)
5. Burghal, D., Ravi, A.T., Rao, V., Alghafis, A.A., Molisch, A.F.: A comprehensive survey of machine learning based localization with wireless signals (2020)
6. Cheng, L., Wu, C., Zhang, Y., Wu, H., Li, M., Maple, C.: A survey of localization in wireless sensor network. *International Journal of Distributed Sensor Networks* **2012** (12 2012)
7. Choi, W., Chang, Y.S., Jung, Y., Song, J.: Low-power lora signal-based outdoor positioning using fingerprint algorithm. *ISPRS International Journal of Geo-Information* **7**(11) (2018)
8. Dargie, W., Poellabauer, C.: *Fundamentals of Wireless Sensor Networks: Theory and Practice*. John Wiley & Sons (2010)
9. Enrico, A., Redondi, C.: Radio Map Interpolation Using Graph Signal Processing. *IEEE Communications Letters* **22**(1), 153–156 (2018)
10. Fan, X., He, X., Xiang, C., Puthal, D., Gong, L., Nanda, P., Fang, G.: Towards system implementation and data analysis for crowdsensing based outdoor RSS maps. *IEEE Access* **6**, 47535–47545 (2018)
11. Ho, K., Gilbert, A., Jin, H., Collomosse, J.: Neural architecture search for deep image prior (2020)
12. Jin, H., Song, Q., Hu, X.: Auto-keras: An efficient neural architecture search system. In: *Proceedings of the 25th ACM SIGKDD*. pp. 1946–1956 (2019)
13. Khelifi, F., Bradai, A., Benslimane, A., Rawat, P., Atri, M.: A Survey of Localization Systems in Internet of Things. *Mobile Networks and Applications* **24**(3), 761–785 (Jun 2019)
14. Krithara, A., Amini, M.R., Renders, J.M., Goutte, C.: Semi-supervised document classification with a mislabeling error model. In: *30th European Conference on Information Retrieval*. pp. 370–381. Glasgow (2008)
15. Kubota, R., Tagashira, S., Arakawa, Y., Kitasuka, T., Fukuda, A.: Efficient survey database construction using location fingerprinting interpolation. In: *2013 IEEE 27th International Conference on Advanced Information Networking and Applications (AINA)*. pp. 469–476 (2013)
16. Laaraiedh, M., Uguen, B., Stephan, J., Corre, Y., Lostanlen, Y., Raspopoulos, M., Stavrou, S.: Ray tracing-based radio propagation modeling for indoor localization purposes. In: *2012 IEEE 17th International Workshop on Computer Aided Modeling and Design of Communication Links and Networks (CAMAD)*. pp. 276–280 (2012)
17. Levie, R., Yapar, V., Kutyniok, G., Caire, G.: Pathloss prediction using deep learning with applications to cellular optimization and efficient d2d link scheduling. In: *ICASSP*. pp. 8678–8682 (2020)
18. Li, J., D.Heap, A.: A review of comparative studies of spatial interpolation methods in environmental sciences: Performance and impact factors. *Ecological Informatics* **6**(3), 228 – 241 (2011)

19. Li, Y., Song, L., Chen, Y., Li, Z., Zhang, X., Wang, X., Sun, J.: Learning dynamic routing for semantic segmentation (2020)
20. Liao, J., Qi, Q., Sun, H., Wang, J.: Radio environment map construction by kriging algorithm based on mobile crowd sensing. *Wireless Communications and Mobile Computing* **2019**, 1–12 (02 2019)
21. Liu, C., Chen, L.C., Schroff, F., Adam, H., Hua, W., Yuille, A.L., Fei-Fei, L.: Auto-deeplab: Hierarchical neural architecture search for semantic image segmentation. In: *Proceedings of CVPR*. pp. 82–92 (2019)
22. Liu, H., Simonyan, K., Yang, Y.: Darts: Differentiable architecture search. *arXiv preprint arXiv:1806.09055* (2018)
23. Ning, C., et al.: Outdoor location estimation using received signal strength-based fingerprinting. *Wireless Pers Commun* **99**, 365–384 (2016)
24. Oliver, M., Webster, R.: Kriging: a method of interpolation for geographical information systems. *International Journal of Geographical Information System* **4**(3), 313–332 (1990)
25. Raspopoulos, M., Laoudias, C., Kanaris, L., Kokkinis, A., Panayiotou, C.G., Stavrou, S.: 3d ray tracing for device-independent fingerprint-based positioning in wlan. In: *2012 9th Workshop on Positioning, Navigation and Communication*. pp. 109–113 (2012)
26. Real, E., Aggarwal, A., Huang, Y., Le, Q.V.: Regularized evolution for image classifier architecture search. In: *AAAI*. vol. 33, pp. 4780–4789 (2019)
27. Redondi, A.E.C.: Radio map interpolation using graph signal processing. *IEEE Communications Letters* **22**(1), 153–156 (2018)
28. Ronneberger, O., P.Fischer, Brox, T.: U-net: Convolutional networks for biomedical image segmentation. In: *Medical Image Computing and Computer-Assisted Intervention (MICCAI)*. LNCS, vol. 9351, pp. 234–241. Springer (2015)
29. Rusu, V., Rusu, C.: Radial Basis Functions Versus Geostatistics in Spatial Interpolations. vol. 217 (10 2006)
30. Sato, K., Inage, K., Fujii, T.: On the performance of neural network residual kriging in radio environment mapping. *IEEE Access* **7**, 94557–94568 (2019)
31. Sorour, S., Lostanlen, Y., Valaee, S., Majeed, K.: Joint indoor localization and radio map construction with limited deployment load. *IEEE Transactions on Mobile Computing* **14**(5), 1031–1043 (2015)
32. Tahat, A., Kaddoum, G., Yousefi, S., Valaee, S., Gagnon, F.: A look at the recent wireless positioning techniques with a focus on algorithms for moving receivers. *IEEE Access* **4**, 6652–6680 (2016)
33. Ulyanov, D., Vedaldi, A., Lempitsky, V.: Deep image prior. *CoRR abs/1711.10925* (2017)
34. Vo, Q.D., De, P.: A Survey of Fingerprint-Based Outdoor Localization. *IEEE Communications Surveys & Tutorials* **18**(1), 491–506 (2016)
35. Wilcoxon, F.: Individual comparisons by ranking methods. *Biometrics* **1**(6), 80–83 (1945)
36. Yu, K., Sharp, I., Guo, Y.: *Ground-Based Wireless Positioning*. John Wiley & Sons, Ltd (06 2009)
37. Zhu, D., Cheng, X., Zhang, F., Yao, X., Gao, Y., Liu, Y.: Spatial interpolation using conditional generative adversarial neural networks. *International Journal of Geographical Information Science* **34**(4), 735–758 (2020)
38. Zoph, B., Le, Q.V.: Neural architecture search with reinforcement learning. *arXiv preprint arXiv:1611.01578* (2016)